

Spatially Resolved Conductivity of Rectangular Interconnects considering Surface Scattering - Part I: Physical Modeling

Xinkang Chen, and Sumeet Kumar Gupta, Senior *Member*, IEEE

Abstract— Accurate modeling of interconnect conductivity is important for performance evaluation of chips in advanced technologies. Surface scattering in interconnects is usually treated by using Fuchs-Sondheimer (FS) approach. While the FS model offer explicit inclusion of the physical parameters, it lacks spatial dependence of conductivity across the interconnect cross-section. To capture the space-dependency of conductivity, an empirical modeling approach based on “cosh” function has been proposed, but it lacks physical insights. In this work, we present a 2D spatially resolved FS (SRFS) model for rectangular interconnects derived from the Boltzmann transport equations. The proposed SRFS model for surface scattering offers both spatial dependence and explicit relation of conductivity to physical parameters such as mean free path and specularly of electrons and interconnect geometry. We highlight the importance of physics-based spatially resolved conductivity model by showing the differences in the spatial profiles between the proposed physical approach and the previous empirical approach. In Part II of this work, we build upon the SRFS approach to propose a compact model for spatially-resolved conductivity accounting for surface scattering in rectangular interconnects.

Index Terms—Boltzmann transport equation, Fuchs-Sondheimer, interconnect, 2D resistivity model

I. INTRODUCTION

Technology scaling has been amongst the most important drivers for the advancement of electronic devices, leading to continual improvements in their speed, energy efficiency and integration density. However, technology scaling comes with its own set of challenges and therefore, mandates innovations to counter them. At the device level, scalable transistor topologies such as FinFETs and nano-sheet transistors [1], [2] are being explored that can manage short channel effects at miniaturized dimensions and provide high transistor performance and energy efficiency. With the transistor designs continually improving, a major bottleneck for technology scaling has emerged in the interconnect design [3].

The challenges in the interconnect scaling are manifold. Reducing the interconnect pitch and width increases their resistance due to lower cross-sectional area (A_w) across which the current conduction takes place. But, more importantly, the resistivity (ρ_w) also increases with width scaling due to increase in the sidewall scattering [4]. Both these factors increase the resistance per unit length for the line metals ($r_{METAL} = \rho_w / A_w$) as well as the resistance of the vias (R_{VIA}). This issue is further aggravated in standard interconnect topologies which utilize thin barrier and/or liner layers to mitigate the electromigration in copper (Cu) [5], [6]. The barrier/liner layers do not scale proportionally with technology scaling, leading to the active conduction area that is lower than the footprint of the interconnects. This, in turn, further increases the sidewall scattering. To counter this, alternate interconnect materials (that can be utilized with thinner or no barrier/liner layers) [7], [8], [9], novel liner/barrier materials (that offer effective barrier functionalities at ultra-thin dimensions) [10] and more scalable interconnect topologies are being explored [11].

To understand the relative pros and cons of various interconnect materials and topologies (that drive their adoption in a technology), modeling their conductivity is highly important. To that end, several modeling approaches have been proposed before. The sidewall scattering is usually treated using the well-known Fuchs-Sondheimer (FS) theory [12]. Another important scattering mechanism due to grain boundaries is captured using the Mayadas-Shatzkes (MS) theory [13]. With these theories forming the bedrock of conductivity modeling, several other works have utilized variants of FS and MS models to estimate the conductivity in scaled technologies [14], [15],

[16]. However, one limitation of the sidewall scattering models in most of the existing works is that the conductivity is not spatially resolved but is an average value across the whole cross section [17]. While this limitation is not that significant for the characterization of thin films or modeling wires with ideal geometries (which was the main target of the previous works [17], [18]), modern interconnect structures need models that can predict the spatially dependent conductivity. One reason for this is that the lithography, etching and deposition of the interconnects lead to a tapered structure [19], with wider width at the top and narrower width at the bottom. As a result, the vertical current path in the vias is non-trivial, especially in the presence of the barrier/liner layers, as shown in Fig. 1. The current spreading [16] necessitates the understanding of how conductivity is distributed across the cross-section.

A notable exception to various interconnect modeling works that does consider the spatial dependence of conductivity accounting for sidewall scattering is [20]. In this work, the authors use an empirical approach using a ‘‘cosh’’ function to model the conductivity as a function of the x - and y - location in the cross-sectional area of the interconnect. However, being an empirical approach, this technique lacks the physical insights that the FS theory provides.

In this two-part paper, we bridge the gap between the FS approach and the ‘‘cosh’’-based model in [20] by obtaining a spatially resolved model for interconnect conductivity while retaining the physical insights of the FS model. In Part I, we derive the spatial dependence of the conductivity of rectangular/square wires (such as vias) based on the FS theory. Based on this, in Part II, we present a compact model for interconnect conductivity considering sidewall scattering and accounting for spatial dependence as well as the dependence on physical parameters. The main contributions of Part I of this work are summarized as follows:

- We derive a generic expression for spatially resolved conductivity of rectangular interconnects based on Boltzmann transport equation (BTE).
- We model the spatially-resolved conductivity as a function of the physical parameters such as specularly

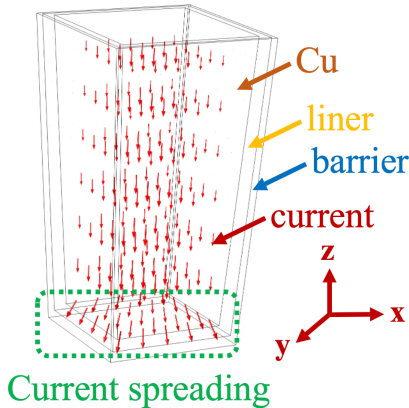


Fig. 1. Tapered via structure with copper conductor and barrier/liner, showing non-trivial current transport (such as current spreading effect at the bottom of the via).

of sidewall scattering (p) and electron mean free path (λ_0).

- We compare the proposed model with the previous ‘‘cosh’’-based modeling approach [20], highlighting the importance of the spatial resolution of conductivity and laying the groundwork for Part II of this paper.

II. BACKGROUND

A. Fuchs-Sondheimer (FS) theory

The Fuchs-Sondheimer (FS) [12] theory is the most popular approach to model the effect of surface scattering on the conductivity of metals based on the Boltzmann transport equation (BTE). In this section, we provide a brief overview of the FS approach.

Let us start with BTE for quasi-free electrons, which, in the presence of an electric field (E) can be written as (1):

$$-\frac{q\vec{E}}{m_{eff}} \cdot \nabla_v f + \vec{v} \cdot \nabla_r f = -\frac{f - f_0}{\tau} \quad (1)$$

Here, f and f_0 are the general and equilibrium distribution functions of the electrons, respectively, q is the electronic charge, m_{eff} is the effective mass of the electrons, v is the electronic velocity, τ is the relaxation time, ∇_v is the gradient operator with respect to v and ∇_r represents the spatial gradient operator.

The solution of (1) can be used to obtain the current density J as

$$\vec{J} = -2q \left(\frac{m_{eff}}{h}\right)^3 \int \vec{v} f d\vec{v} = -2q \left(\frac{m_{eff}}{h}\right)^3 \int \vec{v} \Delta f d\vec{v} \quad (2)$$

where h is the Planck’s constant and $\Delta f = f - f_0$ is the deviation of the electron distribution function from its equilibrium value.

1) Thin Films

For the thin film conductivity considering surface scattering, the approach in [17] utilized (1) and (2) to analyze a metal film of thickness a along with z -direction with E -field in, say, x direction (E_x) – Fig. 2. For a purely diffusive surface scattering, Δf (from (1)) is obtained as

$$\begin{aligned} \Delta f^+ &= \frac{q\tau E_x}{m_{eff}} \frac{\partial f_0}{\partial v_x} \left(1 - e^{-\frac{z}{\tau v_z}}\right) & \text{for } v_z > 0 \\ \Delta f^- &= \frac{q\tau E_x}{m_{eff}} \frac{\partial f_0}{\partial v_x} \left(1 - e^{-\frac{a-z}{\tau v_z}}\right) & \text{for } v_z < 0 \end{aligned} \quad (3)$$

Here, v_z and v_x represent the components of the electron velocity along the film thickness (z) and along the electric field (x); and Δf^+ and Δf^- are for electrons with $v_z > 0$ and $v_z < 0$,

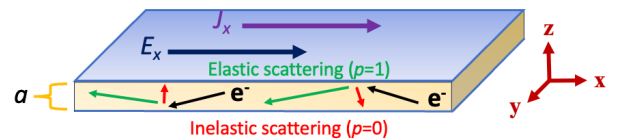


Fig. 2. Thin film structure used for modeling showing fully elastic (specularity $p=1$) or inelastic scattering ($p=0$) when electron hits the top and bottom surfaces.

> REPLACE THIS LINE WITH YOUR MANUSCRIPT ID NUMBER (DOUBLE-CLICK HERE TO EDIT) <

respectively. Using (2) and (3), the current density (J_x) can be calculated as

$$J_x(z) = -\frac{2q^2 m_{eff}^2 E_z}{h^3} \int_0^\infty dv \int_0^{2\pi} \tau v^3 \cos^2(\Phi) \frac{\partial f_0}{\partial v} d\Phi \times \left[\int_0^{\pi/2} \sin^3(\theta) \left(1 - e^{-\frac{z}{\tau v \cos(\theta)}}\right) d\theta + \int_{\pi/2}^\pi \sin^3(\theta) \left(1 - e^{-\frac{a-z}{\tau v \cos(\theta)}}\right) d\theta \right] \quad (4)$$

Here, the spherical coordinates have been used: $v = |\vec{v}|$; $v_z = v \cos(\theta)$; $v_x = v \sin(\theta) \cos(\Phi)$;

Next, a degenerate electron gas is assumed, which implies that for any function $g(v)$, the following holds.

$$\int_0^\infty g(v) \frac{\partial f_0}{\partial v} dv = -g(\tilde{v}) \quad (5)$$

Here, \tilde{v} is the electron velocity at the Fermi surface.

Note, the scattering rate (τ) and \tilde{v} are related to the mean free path of the electrons (λ_0) by

$$\lambda_0 = \tau \tilde{v} \quad (6)$$

Using (5) and (6) in (4), dividing J_x by E_x and averaging along the z -direction, average conductivity accounting for surface scattering can be obtained.

$$\sigma = \frac{1}{a E_x} \int_0^a J_x(z) dz = \sigma_0 \left[1 - \frac{3\lambda_0}{2a} \int_0^{\pi/2} \sin^3(\theta) \cos(\theta) \left(1 - e^{-\frac{a}{\lambda_0 \cos(\theta)}}\right) d\theta \right] \quad (7)$$

Here, σ_0 is the bulk conductivity given by

$$\sigma_0 = \frac{8\pi q^2 m_{eff}^2 \tilde{v}^2}{3 h^3} \lambda_0 \quad (8)$$

A general expression for the conductivity considering both inelastic (diffusive) and elastic (specular) scattering at the surfaces has also been derived in [17]. For this, specularity (p) is defined as the fraction of electrons that are scattered elastically. For this general case, (3) is modified to

$$\Delta f^+ = \frac{q\tau E_x}{m_{eff}} \frac{\partial f_0}{\partial v_x} \left(1 - \frac{1-p}{1-p e^{-a/\tau v_x}} e^{-\frac{z}{\tau v_x}}\right) \quad \text{for } v_z > 0 \quad (9)$$

$$\Delta f^- = \frac{q\tau E_x}{m_{eff}} \frac{\partial f_0}{\partial v_x} \left(1 - \frac{1-p}{1-p e^{a/\tau v_x}} e^{-\frac{a-z}{\tau v_x}}\right) \quad \text{for } v_z < 0$$

Following the same procedure as before, the conductivity is obtained as

$$\sigma = \sigma_0 \left[1 - \frac{3\lambda_0}{2a} (1-p) \int_0^{\pi/2} \frac{\sin^3(\theta) \cos(\theta) \left(1 - e^{-\frac{a}{\lambda_0 \cos(\theta)}}\right)}{1 - p e^{-\frac{a}{\lambda_0 \cos(\theta)}}} d\theta \right] \quad (10)$$

The authors in [17] also derive simplified expressions for (7) and (10) for various limiting conditions (such as $a \ll \lambda_0$ and $a \gg \lambda_0$), which have been utilized by many subsequent works [14], [15], [21].

2) Wire with square cross-section

Following the FS theory, the authors in [18] have derived the conductivity considering surface scattering in square wires. In this case, let us assume that the electric field and the current flow is along the z -direction and the wire has width = a and height = $b=a$ (along the x - and y - directions, respectively) – Fig. 3. Accounting for scattering for the four surfaces of the wire, the following expressions are obtained for Δf considering purely diffusive scattering ($p=0$).

$$\Delta f^{++} = \frac{q\tau E_z}{m_{eff}} \frac{\partial f_0}{\partial v_z} \left(1 - e^{-\frac{\min(\frac{x}{v_x}, \frac{y}{v_y})}{\tau}}\right) \quad \text{for } v_x > 0, v_y > 0$$

$$\Delta f^{-+} = \frac{q\tau E_z}{m_{eff}} \frac{\partial f_0}{\partial v_z} \left(1 - e^{-\frac{\min(\frac{x-a}{v_x}, \frac{y}{v_y})}{\tau}}\right) \quad \text{for } v_x < 0, v_y > 0$$

$$\Delta f^{+-} = \frac{q\tau E_z}{m_{eff}} \frac{\partial f_0}{\partial v_z} \left(1 - e^{-\frac{\min(\frac{x}{v_x}, \frac{y-a}{v_y})}{\tau}}\right) \quad \text{for } v_x > 0, v_y < 0$$

$$\Delta f^{--} = \frac{q\tau E_z}{m_{eff}} \frac{\partial f_0}{\partial v_z} \left(1 - e^{-\frac{\min(\frac{x-a}{v_x}, \frac{y-a}{v_y})}{\tau}}\right) \quad \text{for } v_x < 0, v_y < 0 \quad (11)$$

Here, the first and the second signs on the subscript of Δf represent the direction of x - and y - components of the electron velocity (v_x and v_y), respectively. Using (11) in (2) and following the process as for the thin wires, the authors in [18] obtain the expression for the conductivity averaged over the cross-sectional area as

$$\sigma = \frac{1}{a^2 E_z} \int_0^a \int_0^a J_z(x, y) dx dy = \sigma_0 \left[1 - \frac{2 \int_{v_y > v_x > 0} v_z^2 \left\{ c_1 + c_2 e^{-\frac{a}{\tau v_y}} \right\} d\vec{v}}{\int_{v_x > 0, v_y > 0} v_z^2 d\vec{v}} \right] \quad (12)$$

where

$$c_1 = \frac{\tau v_x}{a} + \frac{\tau v_y}{a} - 2 \frac{\tau v_x \tau v_y}{a} \quad (13)$$

$$c_2 = \frac{\tau v_x}{a} - \frac{\tau v_y}{a} + 2 \frac{\tau v_x \tau v_y}{a}$$

Similar to [17], the authors in [18] derive simplified expressions for various limiting cases (e.g. $a \gg \lambda_0$, $a > 4\lambda_0$, $a \ll \lambda_0$, $a \sim \lambda_0$ etc.), which form the basis of surface scattering models in various subsequent works [14], [15], [21], [22]. Some works have also derived simplified expressions for wires with rectangular and circular cross-sections [22], [23], [24].

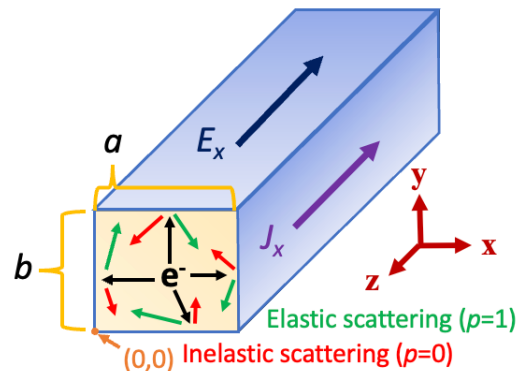


Fig. 3. Rectangular wire structure used for modeling showing fully elastic (specularity $p=1$) or inelastic scattering ($p=0$) when electron hits the four surfaces.

> REPLACE THIS LINE WITH YOUR MANUSCRIPT ID NUMBER (DOUBLE-CLICK HERE TO EDIT) <

B. Spatial Dependence of Conductivity: An Empirical Model

The early fundamental studies of metal conductivity mainly focused on understanding the average behavior of the metal, and hence, the spatial dependence of conductivity was not widely considered. Traditionally, researchers focused on thin film and rectangular wire resistivity without the liner and barrier layers. However, in modern chips, the inclusion of barrier/liner layers in the interconnect structure makes the current transport (especially through the vias) somewhat non-trivial (as discussed before). Despite this, many of the recent works [14], [15], [16] have used the simplified expressions derived from the FS model and utilized fitting parameters to show good match with the experiments. However, one recent work [20] does consider the spatial dependency of the conductivity by modeling the surface scattering effects using an empirical expression. Here, we briefly review some key attributes of this approach.

The resistivity model proposed in [20] shown below employs two terms: the first capturing bulk resistivity and other scattering mechanisms (such as grain boundary scattering) in a lumped parameter ρ_0 , and the second accounting for spatial dependence of resistivity due to surface scattering.

$$\rho(x, y) = \rho_0 + \rho_q \left(\frac{\cosh\left[\frac{x}{\lambda_q}\right]}{\cosh\left[\frac{a}{2\lambda_q}\right]} + \frac{\cosh\left[\frac{y}{\lambda_q}\right]}{\cosh\left[\frac{b}{2\lambda_q}\right]} \right) \quad (14)$$

Here, ρ_q and λ_q are fitting parameters, and a and b are the width and height of the wire cross-section (along the x - and y -directions), respectively. The analysis in [20] shows good match of the average conductivity (obtained by averaging (14) across the cross-section) with the experiments. The main merit of this approach (referred to as the ‘‘cosh’’ model subsequently) is its spatial resolution of resistivity. Using this model, the effect of barrier/liner layers and taper angles can be seamlessly integrated, as in [16]. However, this method does not directly capture the relationship of the conductivity with the physical parameters (such as p , λ_0 etc.).

To address the limitations of the current models, in this paper, we derive the spatial dependence of the conductivity using the FS theory, thereby developing a model that is capable of predicting the relationship of the spatially resolved conductivity with the physical parameters.

III. SPATIALLY RESOLVED FS (SRFS) MODEL FOR RECTANGULAR WIRES

In this section, we present the derivation of the space-dependence of the surface scattering model for rectangular wires following the FS approach, which we refer to as the spatially resolved FS or SRFS model. We start with purely diffusive scatter i.e. specularity (p) = 0. We then generalize the discussion for an arbitrary p (between 0 and 1). We assume that the electric field and the current flow is along the z -direction, and the wire has width and height equal to a and b (along the x - and y - directions), respectively – Fig. 3. For all the discussions in this paper, we assume the origin of the coordinate system to be in the lower left corner of the wire cross-section. (Later on in the paper and in part II, we shift the origin following the symmetry - more on that later).

A. Purely Diffusive Surface Scattering ($p=0$)

Following the same approach as discussed in Section II A for a square wire and accounting for scattering at the four surfaces of the wire, Δf for a rectangular wire is obtained as

$$\begin{aligned} \Delta f^{++} &= \frac{q\tau E_z}{m_{eff}} \frac{\partial f_0}{\partial v_z} \left(1 - e^{-\frac{\min\left(\frac{x}{v_x}, \frac{y}{v_y}\right)}{\tau}} \right) & \text{for } v_x > 0, v_y > 0 \\ \Delta f^{-+} &= \frac{q\tau E_z}{m_{eff}} \frac{\partial f_0}{\partial v_z} \left(1 - e^{-\frac{\min\left(\frac{x-a}{v_x}, \frac{y}{v_y}\right)}{\tau}} \right) & \text{for } v_x < 0, v_y > 0 \\ \Delta f^{+-} &= \frac{q\tau E_z}{m_{eff}} \frac{\partial f_0}{\partial v_z} \left(1 - e^{-\frac{\min\left(\frac{x}{v_x}, \frac{y-b}{v_y}\right)}{\tau}} \right) & \text{for } v_x > 0, v_y < 0 \\ \Delta f^{--} &= \frac{q\tau E_z}{m_{eff}} \frac{\partial f_0}{\partial v_z} \left(1 - e^{-\frac{\min\left(\frac{x-a}{v_x}, \frac{y-b}{v_y}\right)}{\tau}} \right) & \text{for } v_x < 0, v_y < 0 \end{aligned} \quad (15)$$

In order to retain the spatial dependency of the conductivity, the current density ($J_z(x, y)$) needs to be divided by E_z *without averaging along the width and height directions*. Thus, spatially-resolved conductivity ($\sigma(x, y)$) accounting for surface scattering can be obtained.

$$\begin{aligned} \sigma(x, y) &= -\frac{2q^2 m_{eff}^2}{h^3} \int \frac{\partial f_0}{\partial v} \frac{v_z \tau}{v} \zeta \left(\frac{x}{\tau v_x}, \frac{y}{\tau v_y} \right) dv_x dv_y dv_z \quad (16) \end{aligned}$$

Here ζ is a function that depends on the spatial location (x and y) and the electron velocities v_x and v_y and is derived by substituting the four Δf functions of (15) in the expression for J in (2). We will derive the explicit form of this function subsequently.

Transforming the electron velocities to the spherical coordinate system, and following the FS approach (i.e. utilizing the degenerate electron gas condition in (5) and substituting the electron mean free path (λ_0) from (6)), we obtain $\sigma(x, y)$ as

$$\begin{aligned} \sigma(x, y) &= -\frac{2q^2 m_{eff}^2}{h^3} \int_{\theta=0}^{\pi} \int_{\Phi=0}^{2\pi} \tau \tilde{v}^3 \cos^2 \theta \sin \theta \\ &\times \zeta \left(\frac{x}{\lambda_0 \sin \theta \cos \Phi}, \frac{y}{\lambda_0 \sin \theta \sin \Phi} \right) d\Phi d\theta \quad (17) \end{aligned}$$

By substituting bulk conductivity (σ_0) from (8) in (17), we obtain

$$\sigma(x, y) = \frac{3}{4} \sigma_0 \int_{\theta=0}^{\pi} \int_{\Phi=0}^{2\pi} \zeta \left(\frac{x}{\lambda_0 \sin \theta \cos \Phi}, \frac{y}{\lambda_0 \sin \theta \sin \Phi} \right) \cos^2 \theta \sin \theta d\Phi d\theta \quad (18)$$

To simply the ζ function, we consider four cases based on the signs of v_x and v_y (similar to (15)): (i) $v_x > 0, v_y > 0$, for which $\Phi = 0 \rightarrow \frac{\pi}{2}$ and $\Delta f = \Delta f^{++}$, (ii) $v_x < 0, v_y > 0$, ($\Phi = \frac{\pi}{2} \rightarrow \pi$, and $\Delta f = \Delta f^{-+}$), (iii) $v_x > 0, v_y < 0$, ($\Phi = \pi \rightarrow \frac{3\pi}{2}$, and $\Delta f = \Delta f^{+-}$), and (iv) $v_x < 0, v_y < 0$, ($\Phi = \frac{3\pi}{2} \rightarrow 2\pi$, and $\Delta f = \Delta f^{--}$). Thus, the integral of ζ with respect to Φ can be written as

$$\begin{aligned} &\int_{\Phi=0}^{2\pi} \zeta \left(\frac{x}{\lambda_0 \sin \theta \cos \Phi}, \frac{y}{\lambda_0 \sin \theta \sin \Phi} \right) d\Phi \\ &= \int_{\Phi=0}^{\frac{\pi}{2}} \zeta(\Phi)|_{\Delta f = \Delta f^{++}} d\Phi + \int_{\Phi=\frac{\pi}{2}}^{\pi} \zeta(\Phi)|_{\Delta f = \Delta f^{-+}} d\Phi \quad (19) \end{aligned}$$

> REPLACE THIS LINE WITH YOUR MANUSCRIPT ID NUMBER (DOUBLE-CLICK HERE TO EDIT) <

$$+ \int_{\Phi=\pi}^{\frac{3\pi}{2}} \zeta(\Phi)|_{\Delta f = \Delta f^{+-}} d\Phi + \int_{\Phi=\frac{3\pi}{2}}^{2\pi} \zeta(\Phi)|_{\Delta f = \Delta f^{--}} d\Phi$$

We define the four integrals of the right hand side of (19) as $\eta^{++}, \eta^{-+}, \eta^{+-}, \eta^{--}$, respectively, and the left hand side of (19) as η . Thus,

$$\sigma(x, y) = \frac{3}{4} \sigma_0 \int_{\theta=0}^{\pi} \eta(x, y, \theta) \cos^2 \theta \sin \theta d\theta \quad (20)$$

where $\eta(x, y, \theta) = \eta^{++} + \eta^{-+} + \eta^{+-} + \eta^{--}$

Let us first look at η^{++} , it can be observed that the *min* function in (15) dictates that if $\frac{v_y}{v_x} = \frac{v \sin \theta \sin \Phi}{v \sin \theta \cos \Phi} = \tan \Phi < \frac{y}{x}$, Δf^{++} in (15) uses $\left(1 - e^{-\frac{x}{\lambda_0 \sin \theta \cos \Phi}}\right)$, else it uses $\left(1 - e^{-\frac{y}{\lambda_0 \sin \theta \sin \Phi}}\right)$. Thus,

$$\eta^{++} = \int_0^{\tan^{-1}\left(\frac{y}{x}\right)} \left(1 - e^{-\frac{x}{\lambda_0 \sin \theta \cos \Phi}}\right) d\Phi + \int_{\tan^{-1}\left(\frac{y}{x}\right)}^{\frac{\pi}{2}} \left(1 - e^{-\frac{y}{\lambda_0 \sin \theta \sin \Phi}}\right) d\Phi \quad (21a)$$

In a similar manner, when we repeat this for other η functions and change the limits of integration to $0 \rightarrow \frac{\pi}{2}$, we get the following expressions.

$$\eta^{-+} = \int_0^{\tan^{-1}\left(\frac{y}{a-x}\right)} \left(1 - e^{-\frac{a-x}{\lambda_0 \sin \theta \cos \Phi}}\right) d\Phi + \int_{\tan^{-1}\left(\frac{y}{a-x}\right)}^{\frac{\pi}{2}} \left(1 - e^{-\frac{y}{\lambda_0 \sin \theta \sin \Phi}}\right) d\Phi \quad (21b)$$

$$\eta^{+-} = \int_0^{\tan^{-1}\left(\frac{b-y}{x}\right)} \left(1 - e^{-\frac{x}{\lambda_0 \sin \theta \cos \Phi}}\right) d\Phi + \int_{\tan^{-1}\left(\frac{b-y}{x}\right)}^{\frac{\pi}{2}} \left(1 - e^{-\frac{b-y}{\lambda_0 \sin \theta \sin \Phi}}\right) d\Phi \quad (21c)$$

$$\eta^{--} = \int_0^{\tan^{-1}\left(\frac{b-y}{a-x}\right)} \left(1 - e^{-\frac{a-x}{\lambda_0 \sin \theta \cos \Phi}}\right) d\Phi + \int_{\tan^{-1}\left(\frac{b-y}{a-x}\right)}^{\frac{\pi}{2}} \left(1 - e^{-\frac{b-y}{\lambda_0 \sin \theta \sin \Phi}}\right) d\Phi \quad (21d)$$

Substituting (20) in (19), we can rewrite the expression for η as

$$\eta(x, y, \theta) = \sum_{n,d} \left[\int_0^{\tan^{-1}\left(\frac{n}{d}\right)} \left(1 - e^{-\frac{d}{\lambda_0 \sin \theta \cos \Phi}}\right) d\Phi + \int_{\tan^{-1}\left(\frac{n}{d}\right)}^{\frac{\pi}{2}} \left(1 - e^{-\frac{n}{\lambda_0 \sin \theta \sin \Phi}}\right) d\Phi \right] \quad (22)$$

where $(n, d) \rightarrow \{(y, x), (y, a-x), (b-y, x), (b-y, a-x)\}$.

Let us call these four points as the boundary points. Depending on the spatial location, the ascending order of the four boundary points from 0 to $\frac{\pi}{2}$ can have eight different combinations (shown in the Appendix A1). In general, the order of the boundary points may be needed to solve (22), which, being space-dependent, may make the expressions complicated. However, we solve (22) following an approach which makes the order of the breaking points irrelevant and thus considerably simplifies the final SRFS conductivity model. The details of our approach are provided in Appendix A1.

Substituting the simplified expression of (22) in (20), we obtained the final space-dependent conductivity as

$$\sigma(x, y) = \frac{3}{4} \sigma_0 \int_{\theta=0}^{\pi} \eta(x, y, \theta) \cos^2 \theta \sin \theta d\theta \quad (23)$$

$$\eta(x, y, \theta) = 2\pi - 2 \int_{\Phi=0}^{\frac{\pi}{2}} \left\{ e^{-\frac{b}{2\lambda_0 \sin \theta \sin \Phi}} \cosh\left(\frac{y - \frac{b}{2}}{\lambda_0 \sin \theta \sin \Phi}\right) + e^{-\frac{a}{2\lambda_0 \sin \theta \cos \Phi}} \cosh\left(\frac{x - \frac{a}{2}}{\lambda_0 \sin \theta \cos \Phi}\right) \right\} d\Phi - \frac{1}{2} \sum_{n,d} \int_{\Phi=0}^{\frac{\pi}{2}} \left| e^{-\frac{d}{\lambda_0 \sin \theta \cos \Phi}} - e^{-\frac{n}{\lambda_0 \sin \theta \sin \Phi}} \right| d\Phi \quad (24)$$

where $(n, d) \rightarrow \{(y, x), (y, a-x), (b-y, x), (b-y, a-x)\}$ and $x \in [0, a]$, $y \in [0, b]$

B. Specular Surface Scattering (General p)

Let us now generalize the SRFS model accounting for specularity (p) at the surfaces (which, as may be recalled, models both diffusive (inelastic) and elastic scattering at the surface). Here, we consider that all the four surfaces have the same value of p . Following the approach used in [17] for incorporating p in the surface scattering models for thin films (See (9) in Section II), we obtain the expressions for Δf for a rectangular wire.

$$\Delta f^{++} = \frac{q\tau E_z}{m_{eff}} \frac{\partial f_0}{\partial v_z} \left(1 - (1-p) \times \max \left\{ \frac{e^{-\frac{x}{\tau v_x}}}{1-p e^{-a/\tau v_x}}, \frac{e^{-\frac{y}{\tau v_y}}}{1-p e^{-a/\tau v_y}} \right\} \right) \quad \text{for } v_x > 0, v_y > 0$$

$$\Delta f^{-+} = \frac{q\tau E_z}{m_{eff}} \frac{\partial f_0}{\partial v_z} \left(1 - (1-p) \times \max \left\{ \frac{e^{-\frac{x-a}{\tau v_x}}}{1-p e^{a/\tau v_x}}, \frac{e^{-\frac{y}{\tau v_y}}}{1-p e^{-a/\tau v_y}} \right\} \right) \quad \text{for } v_x < 0, v_y > 0$$

$$\Delta f^{+-} = \frac{q\tau E_z}{m_{eff}} \frac{\partial f_0}{\partial v_z} \left(1 - (1-p) \times \max \left\{ \frac{e^{-\frac{x}{\tau v_x}}}{1-p e^{-a/\tau v_x}}, \frac{e^{-\frac{y-b}{\tau v_y}}}{1-p e^{a/\tau v_y}} \right\} \right) \quad \text{for } v_x > 0, v_y < 0$$

$$\Delta f^{--} = \frac{q\tau E_z}{m_{eff}} \frac{\partial f_0}{\partial v_z} \left(1 - (1-p) \times \max \left\{ \frac{e^{-\frac{x-a}{\tau v_x}}}{1-p e^{a/\tau v_x}}, \frac{e^{-\frac{y-b}{\tau v_y}}}{1-p e^{a/\tau v_y}} \right\} \right) \quad \text{for } v_x < 0, v_y < 0 \quad (25)$$

Note, substituting $p=0$ in (25) yields (15) with the *max* function in (25) translating to the *min* of the argument of the exponential function in (15). Following the same process as described in the previous subsection for $p=0$, we obtain the final SRFS conductivity model as a function of specularity (p) as

> REPLACE THIS LINE WITH YOUR MANUSCRIPT ID NUMBER (DOUBLE-CLICK HERE TO EDIT) <

$$\sigma(x, y) = \frac{3}{4} \sigma_0 \int_{\theta=0}^{\pi} \eta(x, y, \theta) \cos^2 \theta \sin \theta d\theta \quad (26)$$

$$\begin{aligned} \eta(x, y, \theta) = & 2\pi - (1-p) \\ & \times \left[2 \int_{\Phi=0}^{\frac{\pi}{2}} \frac{e^{-\frac{a}{2\lambda_0 \sin \theta \cos \Phi}} \times \cosh\left(\frac{x - \frac{a}{2}}{\lambda_0 \sin \theta \cos \Phi}\right)}{1 - p e^{-\frac{a}{\lambda_0 \sin \theta \cos \Phi}}} d\Phi \right. \\ & + 2 \int_{\Phi=0}^{\frac{\pi}{2}} \frac{e^{-\frac{b}{2\lambda_0 \sin \theta \sin \Phi}} \times \cosh\left(\frac{y - \frac{b}{2}}{\lambda_0 \sin \theta \sin \Phi}\right)}{1 - p e^{-\frac{b}{\lambda_0 \sin \theta \sin \Phi}}} d\Phi \\ & + \frac{1}{2} \sum_{n,d} \int_0^{\frac{\pi}{2}} \left| \frac{e^{-\frac{d}{\lambda_0 \sin \theta \cos \Phi}}}{1 - p e^{-\frac{a}{2\lambda_0 \sin \theta \cos \Phi}}} \right. \\ & \left. - \frac{e^{-\frac{n}{\lambda_0 \sin \theta \sin \Phi}}}{1 - p e^{-\frac{b}{2\lambda_0 \sin \theta \sin \Phi}}} \right| d\Phi \end{aligned} \quad (27)$$

where $(n, d) \rightarrow \{(y, x), (y, a - x), (b - y, x), (b - y, a - x)\}$ and $x \in [0, a]$, $y \in [0, b]$

The first term in (27) corresponds to the bulk conductivity and the rest of the terms to surface scattering. Separating the two components, we can write

$$\begin{aligned} \sigma(x, y) = & \sigma_0 - \sigma_{SR}(x, y) \\ = & \sigma_0 - \frac{3}{4} \sigma_0 \int_{\theta=0}^{\pi} \Delta \eta(x, y, \theta) \cos^2 \theta \sin \theta d\theta \end{aligned} \quad (28)$$

$$\begin{aligned} \Delta \eta(x, y, \theta) = & (1-p) \\ & \times \left[2 \int_{\Phi=0}^{\frac{\pi}{2}} \frac{e^{-\frac{a}{2\lambda_0 \sin \theta \cos \Phi}} \times \cosh\left(\frac{x - \frac{a}{2}}{\lambda_0 \sin \theta \cos \Phi}\right)}{1 - p e^{-\frac{a}{2\lambda_0 \sin \theta \cos \Phi}}} d\Phi \right. \\ & + 2 \int_{\Phi=0}^{\frac{\pi}{2}} \frac{e^{-\frac{b}{2\lambda_0 \sin \theta \sin \Phi}} \times \cosh\left(\frac{y - \frac{b}{2}}{\lambda_0 \sin \theta \sin \Phi}\right)}{1 - p e^{-\frac{b}{2\lambda_0 \sin \theta \sin \Phi}}} d\Phi \\ & + \frac{1}{2} \sum_{n,d} \int_0^{\frac{\pi}{2}} \left| \frac{e^{-\frac{d}{\lambda_0 \sin \theta \cos \Phi}}}{1 - p e^{-\frac{a}{2\lambda_0 \sin \theta \cos \Phi}}} \right. \\ & \left. - \frac{e^{-\frac{n}{\lambda_0 \sin \theta \sin \Phi}}}{1 - p e^{-\frac{b}{2\lambda_0 \sin \theta \sin \Phi}}} \right| d\Phi \end{aligned} \quad (29)$$

where $(n, d) \rightarrow \{(y, x), (y, a - x), (b - y, x), (b - y, a - x)\}$ and $x \in [0, a]$, $y \in [0, b]$

Note in (27), the conductivity components (i.e. bulk (σ_0) and surface scattering (σ_{SR})) are subtracted to obtain the overall conductivity. This is different from some recent empirical works [20] which add the resistivity components rather than subtract the conductivity components. Since the conductivity component subtraction follows from the rigorous FS treatment, that should be a preferred method to combine different mechanisms as opposed to resistivity addition.

As can be observed from (27) and (29), the SRFS model offers (1) the space-dependence of conductivity as well as (2) its explicit relationship to physical parameters p , λ_0 and the wire cross-section width (a) and height (b).

C. Normalization and Origin Shifting

Before we conclude this section, we present a variation of the SRFS model by normalizing the parameters and shifting the origin of the coordinate system that will be useful in Part II.

First, we shift the origin of the coordinate system to the center of the wire (rather than the corner, as done in the previous sub-sections). Thus, the wire cross sectional width is from $-a/2$ to $+a/2$ and its height is from $-b/2$ to $+b/2$. Second, we follow a common practice used to express the FS model in terms of the ratio of the wire width/height and the electron mean free path [17]. For that, we define $\kappa_a = \frac{a}{\lambda_0}$ and $\kappa_b = \frac{b}{\lambda_0}$. We also

normalize x and y as $x_n = \frac{x}{a/2}$ and $y_n = \frac{y}{b/2}$. Hence, x_n and y_n range from -1 to 1. With this, the final expressions for SRFS conductivity are summarized in the top of next page. (It may be noted that when implementing this in software like MATLAB, it is recommended to replace \cosh with its exponential-based representation and combine it with the exponential preceding it).

The expression obtained is generic and can be applied for thin films (of thickness b along the along the y -direction) by setting $\kappa_a \rightarrow \infty$. The model for a thin film simplifies to

$$\begin{aligned} \frac{\sigma_{SRFS}(y_n)}{\sigma_0} = & \frac{3}{4} \int_{\theta=0}^{\pi} \eta(y_n, \theta) * \cos^2 \theta \sin \theta d\theta \\ \eta(y_n, \theta) = & 2\pi - (1-p) \\ & \times 4 \int_{\Phi=0}^{\frac{\pi}{2}} \left(\frac{e^{-\frac{\kappa_b}{2 \sin \theta \sin \Phi}} \times \cosh\left(\frac{\kappa_b \times y_n}{2 \sin \theta \sin \Phi}\right)}{1 - p * e^{-\frac{\kappa_b}{\sin \theta \sin \Phi}}} \right) d\Phi \end{aligned} \quad (30)$$

where $y_n \in \frac{y}{b/2} [-1, 1]$ and $\kappa_b = \frac{b}{\lambda_0}$

IV. ANALYSIS

A. Proposed SRFS Model and Previous FS-based Models

As mentioned before, the previous works have utilized the simplified versions of (12) derived in [18] to model the effect of surface scattering on the conductivity of square wires. Here, we utilize the models from [18] (provided for the reader in the appendix A2) and compare them to the values obtained by averaging the SRFS models across the cross section to validate our approach. The comparison is shown in Fig. 4 illustrating how conductivity increases with increasing κ . In [18], the expressions assume that all electrons experience inelastic surface scattering ($p=0$). It can be observed in Fig. 4 that the

> REPLACE THIS LINE WITH YOUR MANUSCRIPT ID NUMBER (DOUBLE-CLICK HERE TO EDIT) <

Final SRFS model for conductivity accounting for specular surface scattering (the figure of wire schematic along with the coordinate system shown alongside)

$$\frac{\sigma_{SRFS}(x_n, y_n)}{\sigma_0} = \frac{3}{4} \int_{\theta=0}^{\pi} \eta(x_n, y_n, \theta) * \cos^2 \theta \sin \theta d\theta$$

$$\eta(x_n, y_n, \theta) = 2\pi - (1-p) \times \left[2 \int_{\Phi=0}^{\frac{\pi}{2}} \left(\frac{e^{\frac{-\kappa_a}{2\sin\theta\cos\Phi}} \times \cosh\left(\frac{\kappa_a \times x_n}{2\sin\theta\cos\Phi}\right)}{1 - p e^{\frac{-\kappa_a}{\sin\theta\cos\Phi}}} + \frac{e^{\frac{-\kappa_b}{2\sin\theta\sin\Phi}} \times \cosh\left(\frac{\kappa_b \times y_n}{2\sin\theta\sin\Phi}\right)}{1 - p * e^{\frac{-\kappa_b}{\sin\theta\sin\Phi}}}\right) d\Phi \right. \\ \left. + \frac{1}{2} \sum_{n,d} \int_{\Phi=0}^{\frac{\pi}{2}} \left| \frac{e^{\frac{-\kappa_a \times d}{2 * \sin\theta\cos\Phi}}}{1 - p e^{\frac{-\kappa_a}{\sin\theta\cos\Phi}}} - \frac{e^{\frac{-\kappa_b \times n}{2 * \sin\theta\sin\Phi}}}{1 - p * e^{\frac{-\kappa_b}{\sin\theta\sin\Phi}}} \right| d\Phi \right]$$

$$\frac{\sigma_{SRFS}(x_n, y_n)}{\sigma_0} = 1 - \frac{\sigma_{SR}(x_n, y_n)}{\sigma_0} = 1 - \frac{3}{4} \int_{\theta=0}^{\pi} \Delta\eta(x, y, \theta) \cos^2 \theta \sin \theta d\theta$$

$$\Delta\eta(x_n, y_n, \theta) = (1-p) \times \left[2 \int_{\Phi=0}^{\frac{\pi}{2}} \left(\frac{e^{\frac{-\kappa_a}{2\sin\theta\cos\Phi}} \times \cosh\left(\frac{\kappa_a \times x_n}{2\sin\theta\cos\Phi}\right)}{1 - p e^{\frac{-\kappa_a}{\sin\theta\cos\Phi}}} + \frac{e^{\frac{-\kappa_b}{2\sin\theta\sin\Phi}} \times \cosh\left(\frac{\kappa_b \times y_n}{2\sin\theta\sin\Phi}\right)}{1 - p e^{\frac{-\kappa_b}{\sin\theta\sin\Phi}}}\right) d\Phi \right. \\ \left. + \frac{1}{2} \sum_{n,d} \int_{\Phi=0}^{\frac{\pi}{2}} \left| \frac{e^{\frac{-\kappa_a \times d}{2 * \sin\theta\cos\Phi}}}{1 - p e^{\frac{-\kappa_a}{\sin\theta\cos\Phi}}} - \frac{e^{\frac{-\kappa_b \times n}{2 * \sin\theta\sin\Phi}}}{1 - p * e^{\frac{-\kappa_b}{\sin\theta\sin\Phi}}} \right| d\Phi \right]$$

where $(n, d) \rightarrow \{(1 + y_n, 1 + x_n), (1 - y_n, 1 + x_n), (1 + y_n, 1 - x_n), (1 - y_n, 1 - x_n)\}$

$$x_n = \frac{x}{a/2} \in [-1, 1], \quad y_n = \frac{y}{b/2} \in [-1, 1]; \quad \kappa_a = \frac{a}{\lambda_0}, \quad \kappa_b = \frac{b}{\lambda_0}$$

average SRFS model for $p=0$ overlaps with the values in [18], validating the expressions presented in the previous sections. We also show conductivity versus κ for other values of p . As p increases and electrons experience more elastic scattering, the conductivity rises sharply. For large p and large κ , the conductivity is close to the bulk value, as expected.

We also compare the FS model with the average conductivity obtained from the proposed SRFS model for a thin film in Fig. 5. The scatter points are obtained from [17] for p equals to 0 and 0.5. Since our SRFS model is general, we set κ_a to be very large value to simulate a thin film and study the effect of different κ_b . Our SRFS model results matches the results from the original FS model [17] for both p values and wide range of dimensions, which again validates the SRFS model.

B. Proposed SRFS Model versus ‘‘cosh’’ Model

The ‘‘cosh’’ model [20] is another spatially resolved conductivity model which uses fitting parameters to match the average conductivity values obtained from the experiment, as described before. Here, we compare the spatial dependence of conductivity predicted by the proposed SRFS model with the ‘‘cosh’’ model. We use width of 10nm and thickness of 29nm for the interconnect as used in [20]. Further, following the method in [20], we lump the bulk conductivity and the grain boundary scattering component in the first term of (28) in the SRFS model, and use the same value of this lumped parameter as in [20]. We then match the average conductivity from SRFS model to the ‘‘cosh’’ model by sweeping p . Specifically, the ‘‘cosh’’ model reports an average conductivity of 9.8 S/ μm . We found $p = 0.663$ in the SRFS model yielding the same value.

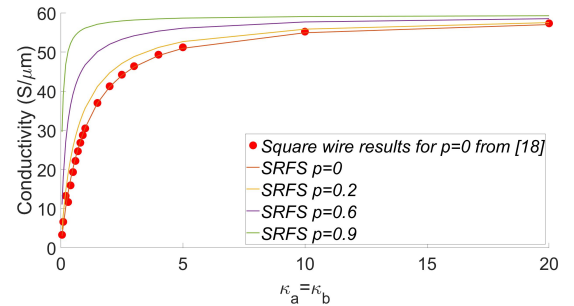
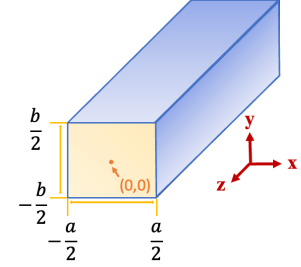


Fig. 4. Conductivity vs κ for different specularity p for a square wire showing the comparison between the proposed SRFS model with the results in [18].

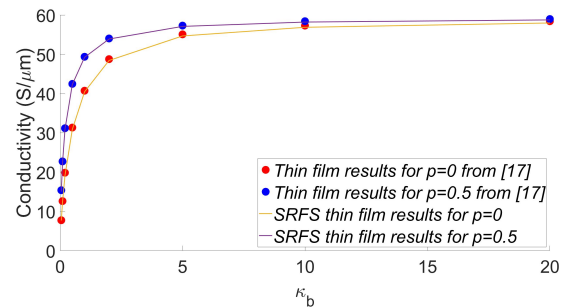


Fig. 5. Conductivity vs κ for different specularity p for a thin film showing the comparison between the proposed SRFS model with the results in [17].

> REPLACE THIS LINE WITH YOUR MANUSCRIPT ID NUMBER (DOUBLE-CLICK HERE TO EDIT) <

After matching the average conductivity, we compare the spatial dependence of conductivity obtained from the two

models. The conductivity along the width (x) direction for $y=0$ and $y=7.25\text{nm}$ are plotted in Fig. 6a and 6b, showing a large

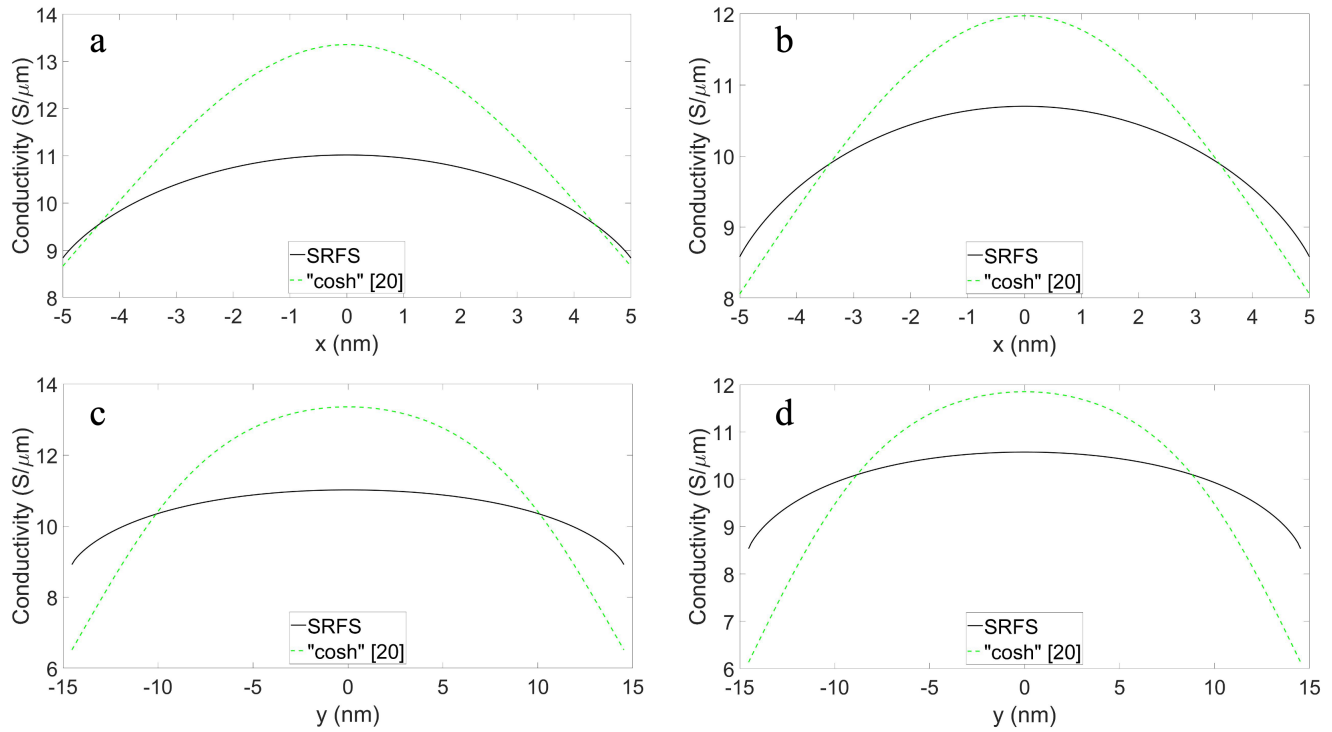


Fig. 6. Conductivity comparison between the proposed SRFS model with “cosh” model along x direction for a) $y=0$ b) $y=7.25\text{nm}$, along y direction for c) $x=0$ d) $x=2.5\text{nm}$, highlighting the mismatch between the proposed physical model and an empirical approach.

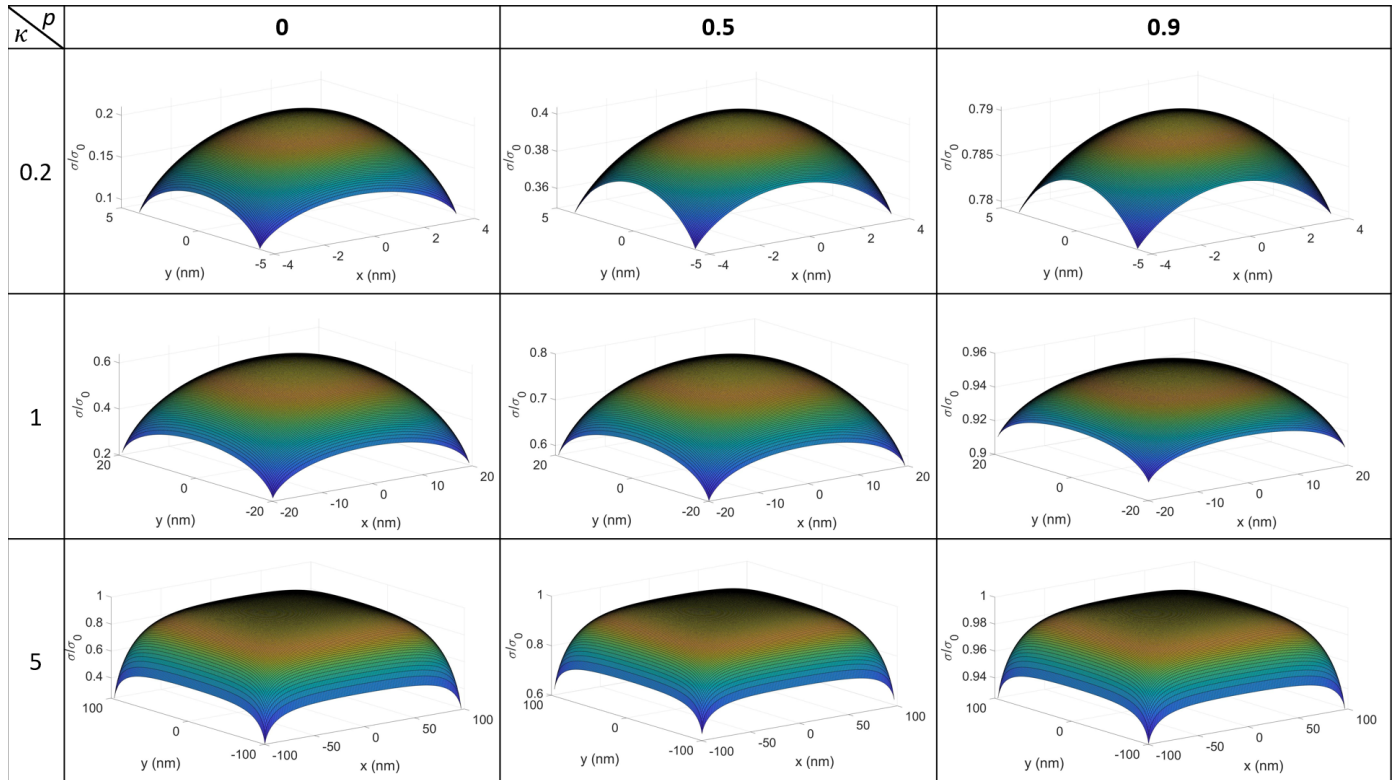


Fig. 7. The spatial profiles for σ/σ_0 (conductivity normalized to bulk conductivity) for different κ and p for a square wire, showing as p increases conductivity also increases, as κ increases conductivity increases to bulk conductivity especially at the center of the wire.

> REPLACE THIS LINE WITH YOUR MANUSCRIPT ID NUMBER (DOUBLE-CLICK HERE TO EDIT) <

mismatch between the physical (SRFS) and the empirical (“cosh”) approaches. Similar mismatches are observed for the conductivity along y in Fig. 6c and 6d. The SRFS model has a much flatter conductivity profile compared to the “cosh” model. Although the average conductivity is the same between the two models, the spatial-dependence of conductivity due to surface scattering shows a significant difference, highlighting the importance for a physics-based spatially resolved conductivity model (such as proposed SRFS approach) as opposed to an empirical approach.

C. SRFS Conductivity for Different κ and p

We show the spatial dependence of conductivity for a square wire predicted by the proposed SRFS model $\kappa=\kappa_a=\kappa_b=0.2, 1, 5$ and $p=0, 0.5, 0.9$ in Fig. 7. At lower κ values, the surface scattering has a larger effect on the conductivity (compared to larger κ), thus, the conductivity is smaller at the center. For small κ , the conductivity reduces smoothly when moving towards the four edges. At larger κ , the surface scattering effect is reduced at the center, so it is closer to bulk conductivity at center. The profile is flat in the center and reduces relatively more sharply closer to the edges (than smaller κ). With an increase in p , the conductivity increases but the shape stays relatively similar.

V. CONCLUSION

We present a 2D spatially resolved FS (SRFS) model for capturing the surface scattering in interconnects with rectangular cross-sections. The primary advantage of our new model is that it offers both space dependence of conductivity and establishes a direct relationship with essential physical parameters. The proposed model is derived from the basic Boltzmann transport equation, which relates the spatially resolved conductivity to electron mean free path, specularity, and the dimensions of the conductor. When compared to the original 1D [17] and 2D FS models [18], the proposed model shows a close match, validating the SRFS expressions derived in this paper. We also show that a previously proposed empirical approach in [20] exhibits a large mismatch in the spatial profile compared to the physics-based modeling approach of SRFS (despite the same average conductivity), highlighting the importance of the latter model presented in this work.

The rigorous nature of the SRFS model leads to complex expressions. While these expressions are easy to implement in standard software such as MATLAB, they may be too time consuming to solve in a circuit simulator. Therefore, building on the SRFS model presented in this part, we present a compact 2D model for spatially resolved conductivity accounting for surface scattering in rectangular interconnects in part II of this work.

$$\eta(x, y, \theta) = \int_{\Phi=0}^{\tan^{-1}(\frac{y}{a-x})} \left\{ \left(1 - e^{-\frac{x}{\lambda_0 \sin \theta \cos \Phi}}\right) + \left(1 - e^{-\frac{a-x}{\lambda_0 \sin \theta \cos \Phi}}\right) + \left(1 - e^{-\frac{x}{\lambda_0 \sin \theta \cos \Phi}}\right) + \left(1 - e^{-\frac{a-x}{\lambda_0 \sin \theta \cos \Phi}}\right) \right\} d\Phi$$

$$+ \int_{\tan^{-1}(\frac{y}{a-x})}^{\tan^{-1}(\frac{y}{x})} \left\{ \left(1 - e^{-\frac{x}{\lambda_0 \sin \theta \cos \Phi}}\right) + \left(1 - e^{-\frac{y}{\lambda_0 \sin \theta \sin \Phi}}\right) + \left(1 - e^{-\frac{x}{\lambda_0 \sin \theta \cos \Phi}}\right) + \left(1 - e^{-\frac{a-x}{\lambda_0 \sin \theta \cos \Phi}}\right) \right\} d\Phi$$

(a1)

APPENDIX A1

In Section III, we discussed the boundary points that define which of the two expressions to use for the “min” function based on the x and y coordinates in (15). When we integrate (22), in general, the order of these boundary points would be needed in the range from 0 to $\frac{\pi}{2}$. If we sort in these boundary points in the ascending order, there are eight different cases depending on the location shown below

$$\begin{aligned} \text{I} : 0 &\rightarrow \frac{y}{a-x} \rightarrow \frac{y}{x} \rightarrow \frac{b-y}{a-x} \rightarrow \frac{b-y}{x} \rightarrow \frac{\pi}{2} \\ \text{II} : 0 &\rightarrow \frac{y}{a-x} \rightarrow \frac{b-y}{a-x} \rightarrow \frac{y}{x} \rightarrow \frac{b-y}{x} \rightarrow \frac{\pi}{2} \\ \text{III} : 0 &\rightarrow \frac{b-y}{a-x} \rightarrow \frac{y}{a-x} \rightarrow \frac{b-y}{a-x} \rightarrow \frac{y}{x} \rightarrow \frac{\pi}{2} \\ \text{IV} : 0 &\rightarrow \frac{b-y}{a-x} \rightarrow \frac{b-y}{x} \rightarrow \frac{y}{a-x} \rightarrow \frac{y}{x} \rightarrow \frac{\pi}{2} \\ \text{V} : 0 &\rightarrow \frac{b-y}{x} \rightarrow \frac{b-y}{a-x} \rightarrow \frac{y}{x} \rightarrow \frac{y}{a-x} \rightarrow \frac{\pi}{2} \\ \text{VI} : 0 &\rightarrow \frac{b-y}{x} \rightarrow \frac{y}{x} \rightarrow \frac{b-y}{a-x} \rightarrow \frac{y}{a-x} \rightarrow \frac{\pi}{2} \\ \text{VII} : 0 &\rightarrow \frac{y}{x} \rightarrow \frac{b-y}{x} \rightarrow \frac{y}{a-x} \rightarrow \frac{b-y}{a-x} \rightarrow \frac{\pi}{2} \\ \text{VIII} : 0 &\rightarrow \frac{y}{x} \rightarrow \frac{y}{a-x} \rightarrow \frac{b-y}{x} \rightarrow \frac{b-y}{a-x} \rightarrow \frac{\pi}{2} \end{aligned}$$

Track all the cases when performing the integration would increase the complexity. To counter this, we describe our approach which averts keeping track of different regions and makes the relative order of the boundary points irrelevant. To illustrate this approach, we take region I in Fig. 8 as an example. For region I, η function can be written as (a1)

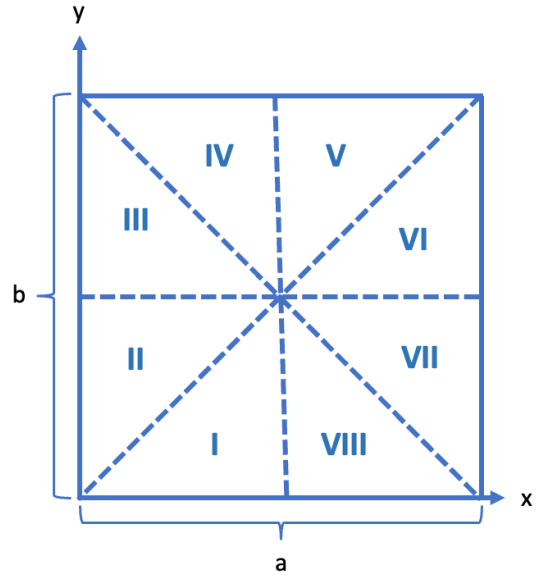


Fig. 8. Wire cross-section showing the eight regions which need to be considered for ordering the boundary points.

> REPLACE THIS LINE WITH YOUR MANUSCRIPT ID NUMBER (DOUBLE-CLICK HERE TO EDIT) <

$$\begin{aligned}
& + \int_{\tan^{-1}(\frac{y}{x})}^{\tan^{-1}(\frac{b-y}{a-x})} \left\{ \left(1 - e^{-\frac{y}{\lambda_0 \sin \theta \sin \Phi}} \right) + \left(1 - e^{-\frac{y}{\lambda_0 \sin \theta \cos \Phi}} \right) + \left(1 - e^{-\frac{x}{\lambda_0 \sin \theta \cos \Phi}} \right) + \left(1 - e^{-\frac{a-x}{\lambda_0 \sin \theta \cos \Phi}} \right) \right\} d\Phi \\
& + \int_{\tan^{-1}(\frac{b-y}{a-x})}^{\tan^{-1}(\frac{b-y}{x})} \left\{ \left(1 - e^{-\frac{y}{\lambda_0 \sin \theta \sin \Phi}} \right) + \left(1 - e^{-\frac{y}{\lambda_0 \sin \theta \cos \Phi}} \right) + \left(1 - e^{-\frac{x}{\lambda_0 \sin \theta \cos \Phi}} \right) + \left(1 - e^{-\frac{b-y}{\lambda_0 \sin \theta \sin \Phi}} \right) \right\} d\Phi \\
& + \int_{\tan^{-1}(\frac{b-y}{x})}^{\frac{\pi}{2}} \left\{ \left(1 - e^{-\frac{y}{\lambda_0 \sin \theta \sin \Phi}} \right) + \left(1 - e^{-\frac{y}{\lambda_0 \sin \theta \cos \Phi}} \right) + \left(1 - e^{-\frac{b-y}{\lambda_0 \sin \theta \sin \Phi}} \right) + \left(1 - e^{-\frac{b-y}{\lambda_0 \sin \theta \cos \Phi}} \right) \right\} d\Phi
\end{aligned} \tag{a1}$$

Equation (a1) can be rewritten as follows by changing the upper limits of all the integrals to $\frac{\pi}{2}$.

$$\begin{aligned}
\eta(x, y, \theta) = & \int_{\Phi=0}^{\frac{\pi}{2}} \left\{ \left(1 - e^{-\frac{x}{\lambda_0 \sin \theta \cos \Phi}} \right) + \left(1 - e^{-\frac{a-x}{\lambda_0 \sin \theta \cos \Phi}} \right) + \left(1 - e^{-\frac{x}{\lambda_0 \sin \theta \cos \Phi}} \right) + \left(1 - e^{-\frac{a-x}{\lambda_0 \sin \theta \cos \Phi}} \right) \right\} d\Phi \\
& - \int_{\Phi=\tan^{-1}(\frac{y}{a-x})}^{\frac{\pi}{2}} \left\{ \left(1 - e^{-\frac{x}{\lambda_0 \sin \theta \cos \Phi}} \right) + \left(1 - e^{-\frac{a-x}{\lambda_0 \sin \theta \cos \Phi}} \right) + \left(1 - e^{-\frac{x}{\lambda_0 \sin \theta \cos \Phi}} \right) + \left(1 - e^{-\frac{a-x}{\lambda_0 \sin \theta \cos \Phi}} \right) \right\} d\Phi \\
& + \int_{\Phi=\tan^{-1}(\frac{y}{a-x})}^{\frac{\pi}{2}} \left\{ \left(1 - e^{-\frac{x}{\lambda_0 \sin \theta \cos \Phi}} \right) + \left(1 - e^{-\frac{y}{\lambda_0 \sin \theta \sin \Phi}} \right) + \left(1 - e^{-\frac{x}{\lambda_0 \sin \theta \cos \Phi}} \right) + \left(1 - e^{-\frac{a-x}{\lambda_0 \sin \theta \cos \Phi}} \right) \right\} d\Phi \\
& - \int_{\Phi=\tan^{-1}(\frac{y}{x})}^{\frac{\pi}{2}} \left\{ \left(1 - e^{-\frac{x}{\lambda_0 \sin \theta \cos \Phi}} \right) + \left(1 - e^{-\frac{y}{\lambda_0 \sin \theta \sin \Phi}} \right) + \left(1 - e^{-\frac{x}{\lambda_0 \sin \theta \cos \Phi}} \right) + \left(1 - e^{-\frac{a-x}{\lambda_0 \sin \theta \cos \Phi}} \right) \right\} d\Phi \\
& + \int_{\Phi=\tan^{-1}(\frac{y}{x})}^{\frac{\pi}{2}} \left\{ \left(1 - e^{-\frac{y}{\lambda_0 \sin \theta \sin \Phi}} \right) + \left(1 - e^{-\frac{y}{\lambda_0 \sin \theta \cos \Phi}} \right) + \left(1 - e^{-\frac{x}{\lambda_0 \sin \theta \cos \Phi}} \right) + \left(1 - e^{-\frac{a-x}{\lambda_0 \sin \theta \cos \Phi}} \right) \right\} d\Phi \\
& - \int_{\Phi=\tan^{-1}(\frac{b-y}{a-x})}^{\frac{\pi}{2}} \left\{ \left(1 - e^{-\frac{y}{\lambda_0 \sin \theta \sin \Phi}} \right) + \left(1 - e^{-\frac{y}{\lambda_0 \sin \theta \cos \Phi}} \right) + \left(1 - e^{-\frac{x}{\lambda_0 \sin \theta \cos \Phi}} \right) + \left(1 - e^{-\frac{a-x}{\lambda_0 \sin \theta \cos \Phi}} \right) \right\} d\Phi \\
& + \int_{\Phi=\tan^{-1}(\frac{b-y}{a-x})}^{\frac{\pi}{2}} \left\{ \left(1 - e^{-\frac{y}{\lambda_0 \sin \theta \sin \Phi}} \right) + \left(1 - e^{-\frac{y}{\lambda_0 \sin \theta \cos \Phi}} \right) + \left(1 - e^{-\frac{x}{\lambda_0 \sin \theta \cos \Phi}} \right) + \left(1 - e^{-\frac{b-y}{\lambda_0 \sin \theta \sin \Phi}} \right) \right\} d\Phi \\
& - \int_{\Phi=\tan^{-1}(\frac{b-y}{x})}^{\frac{\pi}{2}} \left\{ \left(1 - e^{-\frac{y}{\lambda_0 \sin \theta \sin \Phi}} \right) + \left(1 - e^{-\frac{y}{\lambda_0 \sin \theta \cos \Phi}} \right) + \left(1 - e^{-\frac{x}{\lambda_0 \sin \theta \cos \Phi}} \right) + \left(1 - e^{-\frac{b-y}{\lambda_0 \sin \theta \sin \Phi}} \right) \right\} d\Phi \\
& + \int_{\Phi=\tan^{-1}(\frac{b-y}{x})}^{\frac{\pi}{2}} \left\{ \left(1 - e^{-\frac{y}{\lambda_0 \sin \theta \sin \Phi}} \right) + \left(1 - e^{-\frac{y}{\lambda_0 \sin \theta \cos \Phi}} \right) + \left(1 - e^{-\frac{b-y}{\lambda_0 \sin \theta \sin \Phi}} \right) + \left(1 - e^{-\frac{b-y}{\lambda_0 \sin \theta \cos \Phi}} \right) \right\} d\Phi
\end{aligned} \tag{a2}$$

If we observe the second and third expression from (a2), they have the same integration limits and differ from each other only in one of the four sub-expressions. By summing the second and third expressions, we obtain

$$\int_{\tan^{-1}(\frac{y}{a-x})}^{\tan^{-1}(\frac{\pi}{2})} \left(e^{-\frac{y}{\lambda_0 \sin \theta \sin \Phi}} - e^{-\frac{a-x}{\lambda_0 \sin \theta \cos \Phi}} \right) d\Phi \tag{a3}$$

Similarly, adding fourth and fifth expression, we get

$$\int_{\tan^{-1}(\frac{y}{x})}^{\tan^{-1}(\frac{\pi}{2})} \left(e^{-\frac{y}{\lambda_0 \sin \theta \sin \Phi}} - e^{-\frac{x}{\lambda_0 \sin \theta \cos \Phi}} \right) d\Phi \tag{a4}$$

Repeating this for the sixth and seventh expression together yields

$$\int_{\tan^{-1}(\frac{b-y}{a-x})}^{\tan^{-1}(\frac{\pi}{2})} \left(e^{-\frac{b-y}{\lambda_0 \sin \theta \sin \Phi}} - e^{-\frac{a-x}{\lambda_0 \sin \theta \cos \Phi}} \right) d\Phi \tag{a5}$$

Lastly, for the eighth and ninth expression, we get

$$\int_{\tan^{-1}(\frac{b-y}{x})}^{\tan^{-1}(\frac{\pi}{2})} \left(e^{-\frac{b-y}{\lambda_0 \sin \theta \sin \Phi}} - e^{-\frac{x}{\lambda_0 \sin \theta \cos \Phi}} \right) d\Phi \tag{a6}$$

Also, the first expression in (a1) can be rewritten as

$$\begin{aligned}
& 4 \int_{\Phi=0}^{\frac{\pi}{2}} d\Phi - 4 \int_{\Phi=0}^{\frac{\pi}{2}} e^{-\frac{a}{2\lambda_0 \sin \theta \cos \Phi}} \\
& \quad \times \cosh \left(\frac{x-a/2}{\lambda_0 \sin \theta \cos \Phi} \right) d\Phi
\end{aligned} \tag{a7}$$

Combining (a3) - (a7), the η function can be simplified as follow

$$\begin{aligned}
\eta(x, y, \theta) = & 4 \int_{\Phi=0}^{\frac{\pi}{2}} d\Phi \\
& - 4 \int_{\Phi=0}^{\frac{\pi}{2}} e^{-\frac{a}{2\lambda_0 \sin \theta \cos \Phi}} \times \cosh \left(\frac{x-a/2}{\lambda_0 \sin \theta \cos \Phi} \right) d\Phi
\end{aligned} \tag{a8}$$

> REPLACE THIS LINE WITH YOUR MANUSCRIPT ID NUMBER (DOUBLE-CLICK HERE TO EDIT) <

$$\begin{aligned}
& - \left\{ \int_{\tan^{-1}\left(\frac{y}{a-x}\right)}^{\tan^{-1}\left(\frac{\pi}{2}\right)} \left(e^{-\frac{y}{\lambda_0 \sin \theta \sin \Phi}} - e^{-\frac{a-x}{\lambda_0 \sin \theta \cos \Phi}} \right) d\Phi + \int_{\tan^{-1}\left(\frac{y}{x}\right)}^{\tan^{-1}\left(\frac{\pi}{2}\right)} \left(e^{-\frac{y}{\lambda_0 \sin \theta \sin \Phi}} - e^{-\frac{x}{\lambda_0 \sin \theta \cos \Phi}} \right) d\Phi + \right. \\
& \left. \int_{\tan^{-1}\left(\frac{b-y}{a-x}\right)}^{\tan^{-1}\left(\frac{\pi}{2}\right)} \left(e^{-\frac{b-y}{\lambda_0 \sin \theta \sin \Phi}} - e^{-\frac{a-x}{\lambda_0 \sin \theta \cos \Phi}} \right) d\Phi + \int_{\tan^{-1}\left(\frac{b-y}{x}\right)}^{\tan^{-1}\left(\frac{\pi}{2}\right)} \left(e^{-\frac{b-y}{\lambda_0 \sin \theta \sin \Phi}} - e^{-\frac{x}{\lambda_0 \sin \theta \cos \Phi}} \right) d\Phi \right\} \\
& \tag{a8}
\end{aligned}$$

If we look at the terms within the curly bracket, the order of the boundary points does not matter. The expression is only a function of the boundary points. Thus, this η expression holds true for the other seven regions as well.

Recall, when we transformed (a1) to (a2), we make the upper limits of all the integrals to be $\frac{\pi}{2}$ and then combine the expressions. We can also follow a similar process but make the

$$\begin{aligned}
\eta(x, y, \theta) = & \int_{\Phi=0}^{\tan^{-1}\left(\frac{y}{a-x}\right)} \left\{ \left(1 - e^{-\frac{x}{\lambda_0 \sin \theta \cos \Phi}} \right) + \left(1 - e^{-\frac{a-x}{\lambda_0 \sin \theta \cos \Phi}} \right) + \left(1 - e^{-\frac{x}{\lambda_0 \sin \theta \cos \Phi}} \right) + \left(1 - e^{-\frac{a-x}{\lambda_0 \sin \theta \cos \Phi}} \right) \right\} d\Phi \\
& - \int_{\Phi=0}^{\tan^{-1}\left(\frac{y}{a-x}\right)} \left\{ \left(1 - e^{-\frac{x}{\lambda_0 \sin \theta \cos \Phi}} \right) + \left(1 - e^{-\frac{y}{\lambda_0 \sin \theta \sin \Phi}} \right) + \left(1 - e^{-\frac{x}{\lambda_0 \sin \theta \cos \Phi}} \right) + \left(1 - e^{-\frac{a-x}{\lambda_0 \sin \theta \cos \Phi}} \right) \right\} d\Phi \\
& + \int_{\Phi=0}^{\tan^{-1}\left(\frac{y}{x}\right)} \left\{ \left(1 - e^{-\frac{x}{\lambda_0 \sin \theta \cos \Phi}} \right) + \left(1 - e^{-\frac{y}{\lambda_0 \sin \theta \sin \Phi}} \right) + \left(1 - e^{-\frac{x}{\lambda_0 \sin \theta \cos \Phi}} \right) + \left(1 - e^{-\frac{a-x}{\lambda_0 \sin \theta \cos \Phi}} \right) \right\} d\Phi \\
& - \int_{\Phi=0}^{\tan^{-1}\left(\frac{y}{x}\right)} \left\{ \left(1 - e^{-\frac{y}{\lambda_0 \sin \theta \sin \Phi}} \right) + \left(1 - e^{-\frac{y}{\lambda_0 \sin \theta \sin \Phi}} \right) + \left(1 - e^{-\frac{x}{\lambda_0 \sin \theta \cos \Phi}} \right) + \left(1 - e^{-\frac{a-x}{\lambda_0 \sin \theta \cos \Phi}} \right) \right\} d\Phi \\
& + \int_{\Phi=0}^{\tan^{-1}\left(\frac{b-y}{a-x}\right)} \left\{ \left(1 - e^{-\frac{y}{\lambda_0 \sin \theta \sin \Phi}} \right) + \left(1 - e^{-\frac{y}{\lambda_0 \sin \theta \sin \Phi}} \right) + \left(1 - e^{-\frac{x}{\lambda_0 \sin \theta \cos \Phi}} \right) + \left(1 - e^{-\frac{a-x}{\lambda_0 \sin \theta \cos \Phi}} \right) \right\} d\Phi \\
& - \int_{\Phi=0}^{\tan^{-1}\left(\frac{b-y}{a-x}\right)} \left\{ \left(1 - e^{-\frac{y}{\lambda_0 \sin \theta \sin \Phi}} \right) + \left(1 - e^{-\frac{y}{\lambda_0 \sin \theta \sin \Phi}} \right) + \left(1 - e^{-\frac{x}{\lambda_0 \sin \theta \cos \Phi}} \right) + \left(1 - e^{-\frac{b-y}{\lambda_0 \sin \theta \sin \Phi}} \right) \right\} d\Phi \\
& + \int_{\Phi=0}^{\tan^{-1}\left(\frac{b-y}{x}\right)} \left\{ \left(1 - e^{-\frac{y}{\lambda_0 \sin \theta \sin \Phi}} \right) + \left(1 - e^{-\frac{y}{\lambda_0 \sin \theta \sin \Phi}} \right) + \left(1 - e^{-\frac{x}{\lambda_0 \sin \theta \cos \Phi}} \right) + \left(1 - e^{-\frac{b-y}{\lambda_0 \sin \theta \sin \Phi}} \right) \right\} d\Phi \\
& - \int_{\Phi=0}^{\tan^{-1}\left(\frac{b-y}{x}\right)} \left\{ \left(1 - e^{-\frac{y}{\lambda_0 \sin \theta \sin \Phi}} \right) + \left(1 - e^{-\frac{y}{\lambda_0 \sin \theta \sin \Phi}} \right) + \left(1 - e^{-\frac{b-y}{\lambda_0 \sin \theta \sin \Phi}} \right) + \left(1 - e^{-\frac{b-y}{\lambda_0 \sin \theta \sin \Phi}} \right) \right\} d\Phi \\
& + \int_{\Phi=0}^{\frac{\pi}{2}} \left\{ \left(1 - e^{-\frac{y}{\lambda_0 \sin \theta \sin \Phi}} \right) + \left(1 - e^{-\frac{y}{\lambda_0 \sin \theta \sin \Phi}} \right) + \left(1 - e^{-\frac{b-y}{\lambda_0 \sin \theta \sin \Phi}} \right) + \left(1 - e^{-\frac{b-y}{\lambda_0 \sin \theta \sin \Phi}} \right) \right\} d\Phi \\
& \tag{a9}
\end{aligned}$$

lower limit of the integrals to be 0. When we do that, (a1) translates to (a9) in the similar manner as shown below (a9).

By adding first and second, third and fourth, fifth and sixth, and seventh and eighth expressions in pairs together, and

rewriting the ninth expression in terms of cosh (similar to (a7), we can get another expression for η function as below (a10).

For symmetry, we add (a8) and (a10) together and divide by 2 to get the final expression (a11 next page).

Here the n and d define the four boundary points. Note, when we combine (a8) and (a10), we add the two integrals corresponding to the same boundary point in the upper/lower limit of integration to obtain the final integral with $\Phi = 0 \rightarrow \pi/2$. It is noteworthy that the corresponding integrand is the same except for a negative sign. Also, the integrand is always

positive, as dictated by the \min function in (15). Hence, we use the absolute value of $(e^{-\frac{d}{\lambda_0 \sin \theta \cos \Phi}} - e^{-\frac{n}{\lambda_0 \sin \theta \sin \Phi}})$ and combine the integrals to obtain the final expression in (a11). This approach is also valid for a general p .

$$\begin{aligned}
\eta(x, y, \theta) = & 4 \int_{\Phi=0}^{\frac{\pi}{2}} d\Phi - 4 \int_{\Phi=0}^{\frac{\pi}{2}} e^{-\frac{b}{2\lambda_0 \sin \theta \sin \Phi}} \times \cosh\left(\frac{y-b/2}{\lambda_0 \sin \theta \sin \Phi}\right) d\Phi \\
& - \left\{ \int_{\tan^{-1}(0)}^{\tan^{-1}\left(\frac{b-y}{x}\right)} \left(e^{-\frac{x}{\lambda_0 \sin \theta \cos \Phi}} - e^{-\frac{b-y}{\lambda_0 \sin \theta \sin \Phi}} \right) d\Phi + \int_{\tan^{-1}(0)}^{\tan^{-1}\left(\frac{b-y}{a-x}\right)} \left(e^{-\frac{a-x}{\lambda_0 \sin \theta \cos \Phi}} - e^{-\frac{b-y}{\lambda_0 \sin \theta \sin \Phi}} \right) d\Phi \right. \\
& \left. + \int_{\tan^{-1}(0)}^{\tan^{-1}\left(\frac{y}{x}\right)} \left(e^{-\frac{x}{\lambda_0 \sin \theta \cos \Phi}} - e^{-\frac{y}{\lambda_0 \sin \theta \sin \Phi}} \right) d\Phi + \int_{\tan^{-1}(0)}^{\tan^{-1}\left(\frac{y}{a-x}\right)} \left(e^{-\frac{a-x}{\lambda_0 \sin \theta \cos \Phi}} - e^{-\frac{y}{\lambda_0 \sin \theta \sin \Phi}} \right) d\Phi \right\} \\
& \tag{a10}
\end{aligned}$$

> REPLACE THIS LINE WITH YOUR MANUSCRIPT ID NUMBER (DOUBLE-CLICK HERE TO EDIT) <

$$\begin{aligned}
\eta(x, y, \theta) &= 2\pi \\
&- 2 \int_{\Phi=0}^{\frac{\pi}{2}} \left\{ e^{-\frac{b}{2\lambda_0 \sin\theta \sin\Phi}} \times \cosh\left(\frac{y - \frac{b}{2}}{\lambda_0 \sin\theta \sin\Phi}\right) \right. \\
&+ \left. e^{-\frac{a}{2\lambda_0 \sin\theta \cos\Phi}} \times \cosh\left(\frac{x - \frac{a}{2}}{\lambda_0 \sin\theta \cos\Phi}\right) d\Phi \right\} \quad (\text{a11}) \\
&- \frac{1}{2} \sum_{n,d} \int_{\Phi=0}^{\frac{\pi}{2}} \left| e^{-\frac{d}{\lambda_0 \sin\theta \cos\Phi}} - e^{-\frac{n}{\lambda_0 \sin\theta \sin\Phi}} \right| d\Phi
\end{aligned}$$

where $(n, d) \rightarrow \{(y, x), (y, a - x), (b - y, x), (b - y, a - x)\}$

APPENDIX A2

For validating the SRFS model, we use the models from [18] for a square wire (of height=width= a). The authors in [17] have derived various simplified expressions for various κ ($\kappa = a/\lambda_0$), which we utilize for comparison in Fig. 4. We list these approximations from (4) for the convenience of the readers.

$$\frac{\sigma}{\sigma_0} = \frac{3}{4} \kappa \log_e \left(\frac{\sqrt{2+1}}{\sqrt{2-1}} \right) - \frac{1}{2} \kappa (\sqrt{2} - 1) \quad \text{for } \kappa < 0.2 \quad (\text{a12})$$

$$\begin{aligned}
\frac{\sigma}{\sigma_0} &= 1 - \frac{3}{\pi} \left(\frac{\pi}{4\kappa} - \frac{4}{15\kappa^2} \right) \\
&+ \frac{12}{\pi} \int_0^{\frac{\pi}{2}} \left(\frac{\pi \cos\theta}{4\kappa} - \frac{\kappa \sin\theta - \sin 2\theta}{3\kappa^2} \right) e^{-\frac{\kappa}{\cos\theta}} \sin^3 \theta d\theta \\
&+ \frac{12}{\pi} \int_{\frac{\pi}{4}}^{\frac{\pi}{2}} \left(\frac{\cos\theta}{\kappa} \left(\frac{\pi}{4} - \frac{\cos(\cot\theta)^{-1}}{2} \right) + \right. \\
&\left. \frac{\cot^2 \theta}{2\kappa} \sqrt{(-\cos 2\theta)} - \frac{\sin\theta - (-\cos 2\theta)^{3/2} / \sin\theta^2}{3\kappa} \right) e^{-\frac{\kappa}{\cos\theta}} \sin^3 \theta d\theta \\
&\quad \text{for } 0.2 < \kappa < 4
\end{aligned} \quad (\text{a13})$$

$$\begin{aligned}
\frac{\sigma}{\sigma_0} &= 1 - \frac{6}{\pi} \left(\frac{\pi}{8\kappa} - \frac{2}{15\kappa^2} \right) + \\
&\frac{12}{\pi\kappa} \int_{\theta=0}^{\frac{\pi}{2}} \int_{\phi=0}^{\frac{\pi}{4}} e^{\frac{-\kappa}{\sin\theta \cos\phi}} \cos\phi \sin^2 \theta \cos^2 \theta d\theta d\phi + \\
&\frac{12}{\pi\kappa^2} \int_{\theta=0}^{\frac{\pi}{2}} \left(\frac{e^{-\sqrt{2}\kappa/\sin\theta}}{2} - e^{-\kappa/\sin\theta} \right) \sin^3 \theta \cos^2 \theta d\theta \\
&\quad \text{for } \kappa > 4
\end{aligned} \quad (\text{a14})$$

ACKNOWLEDGMENT

This work was supported, in part, by SRC/NIST-funded NEWLIMITS Center (Award number 70NANB17H041)

REFERENCES

[1] B. Yu *et al.*, “FinFET scaling to 10 nm gate length,” in *Digest. International Electron Devices Meeting*, 2002, pp. 251–254. doi: 10.1109/IEDM.2002.1175825.

[2] J. Ajayan *et al.*, “Nanosheet field effect transistors-A next generation device to keep Moore’s law alive: An intensive study,” *Microelectronics J*, vol. 114, p. 105141, 2021.

[3] R. Brain, “Interconnect scaling: Challenges and opportunities,” in *2016 IEEE International Electron Devices Meeting (IEDM)*, 2016, pp. 9.3.1–9.3.4. doi: 10.1109/IEDM.2016.7838381.

[4] R. L. Graham *et al.*, “Resistivity dominated by surface scattering in sub-50 nm Cu wires,” *Appl Phys Lett*, vol. 96, no. 4, 2010, doi: 10.1063/1.3292022.

[5] W. L. Wang *et al.*, “The Reliability Improvement of Cu Interconnection by the Control of Crystallized α -Ta/TaN_x Diffusion Barrier,” *J Nanomater*, vol. 2015, 2015, doi: 10.1155/2015/917935.

[6] D. Edelstein *et al.*, “A high performance liner for copper damascene interconnects,” in *Proceedings of the IEEE 2001 International Interconnect Technology Conference (Cat. No.01EX461)*, 2001, pp. 9–11. doi: 10.1109/IITC.2001.930001.

[7] N. Bekiaris *et al.*, “Cobalt fill for advanced interconnects,” in *2017 IEEE International Interconnect Technology Conference (IITC)*, 2017, pp. 1–3. doi: 10.1109/IITC-AMC.2017.7968981.

[8] D. Wan *et al.*, “Subtractive Etch of Ruthenium for Sub-5nm Interconnect,” in *2018 IEEE International Interconnect Technology Conference (IITC)*, 2018, pp. 10–12. doi: 10.1109/IITC.2018.8454841.

[9] T. M. Philip *et al.*, “First-Principles Evaluation of fcc Ruthenium for its use in Advanced Interconnects,” *Phys Rev Appl*, vol. 13, no. 4, Apr. 2020, doi: 10.1103/PhysRevApplied.13.044045.

[10] C. L. Lo *et al.*, “Opportunities and challenges of 2D materials in back-end-of-line interconnect scaling,” *Journal of Applied Physics*, vol. 128, no. 8. American Institute of Physics Inc., Aug. 28, 2020. doi: 10.1063/5.0013737.

[11] B. Grot, J. Hestness, S. W. Keckler, and O. Mutlu, “Express Cube Topologies for on-Chip Interconnects,” in *2009 IEEE 15th International Symposium on High Performance Computer Architecture*, 2009, pp. 163–174. doi: 10.1109/HPCA.2009.4798251.

[12] E. H. SONDHEIMER, “Influence of a Magnetic Field on the Conductivity of Thin Metallic Films,” *Nature*, vol. 164, no. 4178, pp. 920–921, 1949, doi: 10.1038/164920a0.

[13] A. F. Mayadas and M. Shatzkes, “Electrical-Resistivity Model for Polycrystalline Films: the Case of Arbitrary Reflection at External Surfaces,” *Phys Rev B*, vol. 1, no. 4, pp. 1382–1389, Feb. 1970, doi: 10.1103/PhysRevB.1.1382.

[14] R. Mehta, S. Chugh, and Z. Chen, “Enhanced electrical and thermal conduction in graphene-encapsulated copper nanowires,” *Nano Lett*, vol. 15, no. 3, pp. 2024–2030, Mar. 2015, doi: 10.1021/nl504889t.

[15] T. Shen *et al.*, “MoS₂ for Enhanced Electrical Performance of Ultrathin Copper Films,” *ACS Appl Mater Interfaces*, vol. 11, no. 31, pp. 28345–28351, Aug. 2019, doi: 10.1021/acsami.9b03381.

[16] X. Chen, C.-L. Lo, M. C. Johnson, Z. Chen, and S. K. Gupta, “Modeling and Circuit Analysis of Interconnects with TaS₂ Barrier/Liner,” in *2021 Device Research Conference (DRC)*, 2021, pp. 1–2. doi: 10.1109/DRC52342.2021.9467160.

[17] E. H. Sondheimer, “The mean free path of electrons in metals,” *Adv Phys*, vol. 1, no. 1, pp. 1–42, 1952, doi: 10.1080/00018735200101151.

[18] D. K. C. Macdonald and K. Sarginson, “Size Effect Variation of the Electrical Conductivity of Metals,” 1950. [Online]. Available: <https://about.jstor.org/terms>

[19] T. Lu and A. Srivastava, “Detailed electrical and reliability study of tapered TSVs,” in *2013 IEEE International 3D Systems Integration Conference (3DIC)*, 2013, pp. 1–7. doi: 10.1109/3DIC.2013.6702350.

[20] I. Ciofi *et al.*, “Impact of Wire Geometry on Interconnect RC and Circuit Delay,” *IEEE Trans Electron Devices*, vol. 63, no. 6, pp. 2488–2496, Jun. 2016, doi: 10.1109/TED.2016.2554561.

[21] R. Saligram, S. Datta, and A. Raychowdhury, “Scaled Back End of Line Interconnects at Cryogenic Temperatures,” *IEEE Electron Device Letters*, vol. 42, no. 11, pp. 1674–1677, Nov. 2021, doi: 10.1109/LED.2021.3117277.

[22] J. S. Chawla, F. Gstrein, K. P. O’Brien, J. S. Clarke, and D. Gall, “Electron scattering at surfaces and grain boundaries in Cu thin films and wires,” *Phys Rev B Condens Matter Mater Phys*, vol. 84, no. 23, Dec. 2011, doi: 10.1103/PhysRevB.84.235423.

[23] R. S. Smith *et al.*, “An evaluation of Fuchs-Sondheimer and Mayadas-Shatzkes models below 14nm node wide lines,” *AIP Adv*, vol. 9, no. 2, Feb. 2019, doi: 10.1063/1.5063896.

[24] D. Gall, “The search for the most conductive metal for narrow interconnect lines,” *Journal of Applied Physics*, vol. 127, no. 5. American Institute of Physics Inc., Feb. 07, 2020. doi: 10.1063/1.5133671.